*J. Fluid Mech.* (2025), *vol.* 1012, A12, doi:10.1017/jfm.2025.10216

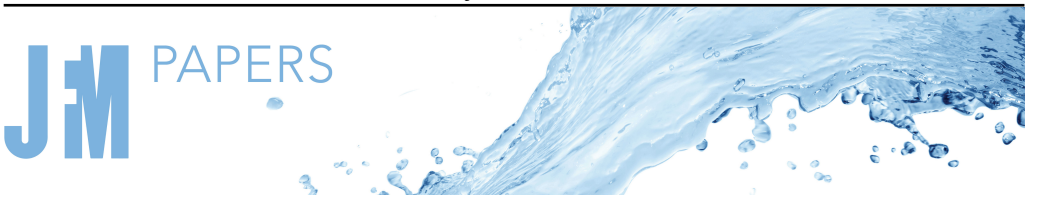

# Large deformation of elastic capsules under uniaxial extensional flow

**Ehud Yariv**[1,2], **Peter D. Howell**[3] and **Howard A. Stone**[2]

[1]Department of Mathematics, Technion – Israel Institute of Technology, Haifa 32000, Israel

[2]Department of Mechanical and Aerospace Engineering, Princeton University, Princeton, NJ 08544, USA

[3]Mathematical Institute, University of Oxford, Oxford OX2 6GG, UK

**Corresponding author:** Ehud Yariv, udi@technion.ac.il

(Received 24 February 2025; revised 24 April 2025; accepted 2 May 2025)

A spherical capsule (radius $R$) is suspended in a viscous liquid (viscosity $\mu$) and exposed to a uniaxial extensional flow of strain rate $E$. The elasticity of the membrane surrounding the capsule is described by the Skalak constitutive law, expressed in terms of a surface shear modulus $G$ and an area dilatation modulus $K$. Dimensional arguments imply that the slenderness $\epsilon$ of the deformed capsule depends only upon $K/G$ and the elastic capillary number $Ca = \mu RE/G$. We address the coupled flow–deformation problem in the limit of strong flow, $Ca \gg 1$, where large deformation allows for the use of approximation methods in the limit $\epsilon \ll 1$. The key conceptual challenge, encountered at the very formulation of the problem, is in describing the Lagrangian mapping from the spherical reference state in a manner compatible with hydrodynamic slender-body formulation. Scaling analysis reveals that $\epsilon$ is proportional to $Ca^{-2/3}$, with the hydrodynamic problem introducing a dependence of the proportionality prefactor upon $\ln\epsilon$. Going beyond scaling arguments, we employ asymptotic methods to obtain a reduced formulation, consisting of a differential equation governing a mapping field and an integral equation governing the axial tension distribution. The leading-order deformation is independent of the ratio $K/G$; in particular, we find the approximation $\epsilon^{2/3}Ca \approx 0.2753\ln(2/\epsilon^2)$ for the relation between $\epsilon$ and $Ca$. A scaling analysis for the neo-Hookean constitutive law reveals the impossibility of a steady slender shape, in agreement with existing numerical simulations. More generally, the present asymptotic paradigm allows us to rigorously discriminate between strain-softening and strain-hardening models.

**Key words:** capsule/cell dynamics, membranes, slender-body theory

## 1. Introduction

Capsules, consisting of a liquid core surrounded by a membrane, are common in both nature (e.g. cells) and bioengineering applications (Pozrikidis 2003*b*). Since the membrane is elastic, it deforms under flow. Due to the possibility of breakup, there is interest in mechanical modelling of deformation (Barthés-Biesel 2016). In particular, the desire to characterise the mechanical properties of cell membranes has led to the development of deformability cytometry (Mietke *et al.* 2015; Otto *et al.* 2015; Rosendahl *et al.* 2018), where cells are subject to shearing flow in microfluidic devices, with their deformation being recorded by high-speed cameras.

It is common to model the thin membrane by a two-dimensional surface with an elastic constitutive law that introduces resistance to shear and area dilatation, but not to bending. The canonical problem involves the specification of simple shear flow, under which the membrane deforms. More generally, other types of linear flows have been considered, in particular two-dimensional elongational flow and axially symmetric hyperbolic flow. In these flows, the capsule shape can reach a steady state (which is unattainable under simple shear). For that reason, such flows are convenient for experimental observations and possibly for characterising material response (Chang & Olbricht 1993). With a steady state, moreover, the internal liquid is stationary, so its viscosity does not play a role.

The deformed shape of the membrane is determined by static equilibrium, where the hydrodynamic tractions are balanced by the (surface divergence of the) elastic stresses. There is a fundamental difference in determining the hydrodynamic and elastic forces. The hydrodynamic problem, and in particular the resulting traction, is determined by the deformed shape alone. The elastic stresses are set by the deformation from a given reference (typically spherical) shape to the present shape. The theoretical calculation of capsule deformation falls under the broader framework of fluid–structure interactions (Dowell & Hall 2001). Given the typical small size of capsules (e.g. approximately 10 $\mu$m for a red blood cell), inertia is typically negligible; the flow is therefore governed by the Stokes equations.

Modelling the elastic response to deformation requires a constitutive law for the stresses. The neo-Hookean law, a particular case of the Mooney–Rivlin law, constitutes the thin limit of an incompressible solid; it appropriately describes rubber-like materials. Another common model is the Skalak law (Skalak *et al.* 1973), an isotropic two-dimensional model with independent surface shear and area dilatation moduli that was specifically designed to model red blood cells. Both constitutive descriptions are nonlinear. With the deformed shape itself being unknown, the equilibrium problem is inherently nonlinear.

The key parameter governing the dimensionless problem is the elastic capillary number $Ca$, representing the characteristic ratio of viscous stresses to elastic stresses. Initial investigations (Barthés-Biesel 1980; Barthés-Biesel & Rallison 1981) considered the stiff limit $Ca \ll 1$, where the membrane deforms only slightly. Given the interest in significant deformations, these were later supplemented by numerical simulations at finite values of $Ca$ (Li, Barthés-Biesel & Helmy 1988; Pozrikidis 1990, 2003*a*; Dodson III & Dimitrakopoulos 2008, 2009). The ultimate goal of the theoretical analysis is the calculation of the capsule deformation; representing it by appropriate lumped scalar measures, it is desirable to understand how they vary as a function of $Ca$.

At large $Ca$ the capsule undergoes large deformation whose nature, as observed numerically, depends critically on the elastic behaviour. For certain constitutive laws, the most notable being neo-Hookean, there exists a critical capillary number beyond which no steady shape is attained under elongation (Li *et al.* 1988). For that reason the

neo-Hookean law is classified as 'strain softening'. For 'strain hardening' laws, such as the Skalak description, the capsule does attain a steady slender shape for large $Ca$ (Li *et al.* 1988; Barthès-Biesel *et al.* 2002; Walter *et al.* 2010). In fact, numerical computations (Dodson III & Dimitrakopoulos 2008, 2009) reveal slender shapes even at moderately large capillary numbers, $Ca \approx 2.5$.

Motivated by the interest in large deformation (Eggleton & Popel 1998; Navot 1998; Ramanujan & Pozrikidis 1998) we conduct here an asymptotic investigation in the limit $Ca \gg 1$. Our key goal is to determine the asymptotic dependence of the slenderness $\epsilon$ upon $Ca$. For simplicity we consider uniaxial extensional flow, where the problem is axially symmetric, and seek the steady shape attained by the capsule.

In classical slender-body analyses about rigid bodies (Batchelor 1970; Cox 1970) the slenderness $\epsilon \ll 1$ is prescribed in the problem formulation. A key challenge in the present problem is that the slenderness is unknown to begin with, and is in fact a part of the problem. In that sense, our problem is reminiscent of bubble deformation (Buckmaster 1972, 1973; Acrivos & Lo 1978; Sherwood 1981). It is, however, significantly more complicated. The free surface in the bubble problem is characterised by a uniform surface tension; consequently, its mechanical model is expressed via an internal force that acts normal to the surface. The membrane of a capsule is described by more elaborate mechanics that result in both normal and tangential internal forces. In that aspect, the present problem is closer to that describing a bubble whose boundary is contaminated by surfactants (Booty & Siegel 2005). Another challenge we face, which seems new in slender-body analyses, has to do with the conflict between the 'Lagrangian' description required for the calculation of the elastic stress and the 'Eulerian' description required for the hydrodynamic formulation.

In analysing the deformation problem at large $Ca$ it is necessary to allow for cusped ends. The transition from spindled-to-cusped edges was originally observed in experiments (Barthés-Biesel 1991) using a four-roller apparatus (e.g. Bentley & Leal 1986). In fact, the inability of 'state of the art' computation schemes (at that time) to reach large capillary numbers, beyond that transition, motivated the use of spectral boundary-element algorithms (Wang & Dimitrakopoulos 2006; Dodson III & Dimitrakopoulos 2008) that do predict cusped ends. In our asymptotic analysis, we allow for pointed ends at the very outset. This affects the boundary conditions governing the deformed shape.

Following the numerical classification of strain softening and strain hardening materials, we employ here the Skalak model which was numerically observed to result in steady-state large deformation. Indeed, it seems that the Skalak model has become the *de facto* constitutive description for capsules in the literature (Dodson III & Dimitrakopoulos 2008, 2009). We also briefly discuss the strain softening neo-Hookean model, which was numerically observed to burst under strong flows.

## 2. Problem formulation

### 2.1. *Physical problem*

A capsule is made of a liquid core and an elastic encapsulating membrane, whose reference shape is spherical, say of radius $R$. The thin membrane is described by an effective two-dimensional elasticity which represents resistance to shear (captured by the modulus $G$) and area dilatation (captured by the modulus $K$), but no resistance to bending. The two material coefficients have the dimensions of surface tension, i.e. force per unit length.

The capsule is suspended in a viscous liquid of viscosity $\mu$ and is exposed to a uniaxial extensional flow of extension rate $E$. The capsule reaches a steady shape whose symmetry

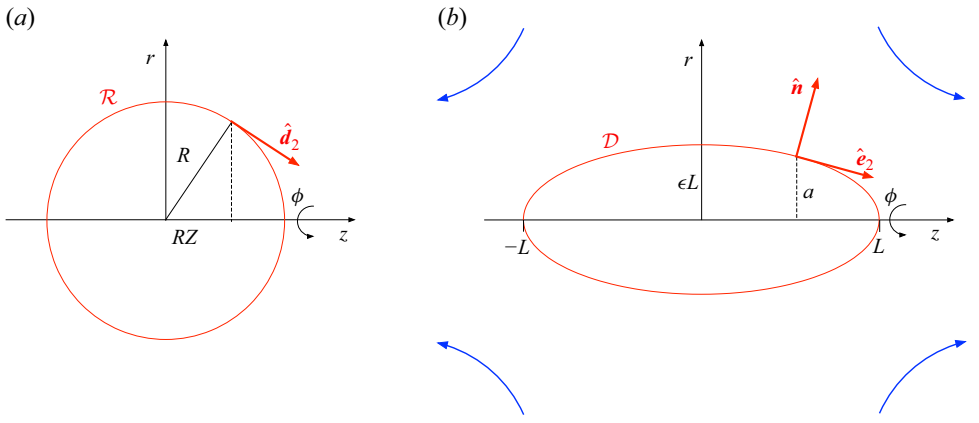


Figure 1. Schematic of the reference (*a*) and deformed (*b*) geometries.

axis is aligned with the axis of extension. The capsule length along that axis is denoted by $2L$; its 'waist' radius in the midway symmetry plane is denoted by $\epsilon L$. Our interest is in the evaluation of the geometric parameters $\epsilon$ and $L/R$, which quantify the overall deformation. By dimensional arguments, these parameters can only depend upon the two dimensionless parameters of the problem, namely $K/G$ and the elastic capillary number

$$Ca = \frac{\mu R E}{G}, \tag{2.1}$$

which expresses the relative magnitude of viscous and elastic stresses. Once the capsule reaches a steady shape, its core liquid is stationary. The ratio of the core viscosity to the external-liquid viscosity – a third dimensionless parameter which affects the transient problem – is accordingly irrelevant.

### 2.2. *Geometry*

We employ cylindrical $(r, \phi, z)$ coordinates with the $z$-axis coinciding with axis of symmetry and $z = 0$ coinciding with the symmetry plane of the extensional flow. We write the shape of the deformed membrane $\mathcal{D}$ as

$$r = a(z), \tag{2.2}$$

see figure 1. Since the deformed shape is symmetric about the plane $z = 0$, $a$ is an even function: $a(-z) = a(z)$. By definition,

$$a(\pm L) = 0. \tag{2.3}$$

Given the definition of $\epsilon$, the shape function also satisfies

$$a(0) = \epsilon L. \tag{2.4}$$

Since the capsule core is incompressible, volume conservation gives the constraint

$$\int_{-L}^{L} a^2(z)\,\mathrm{d}z = \frac{4}{3}R^3. \tag{2.5}$$

Using $z$ and $\phi$ for parametrisation, the position vector pointing to the deformed membrane $\mathcal{D}$ is

$$\boldsymbol{r}(z, \phi) = a(z)\,\hat{\boldsymbol{e}}_r + z\hat{\boldsymbol{e}}_z. \tag{2.6}$$

By differentiating (2.6) we obtain

$$\frac{\partial \boldsymbol{r}}{\partial \phi} = h_1 \hat{\boldsymbol{e}}_1, \quad \frac{\partial \boldsymbol{r}}{\partial z} = h_2 \hat{\boldsymbol{e}}_2, \tag{2.7a,b}$$

where the associated basis vectors and corresponding scale factors are

$$\hat{\boldsymbol{e}}_1 = \hat{\boldsymbol{e}}_\phi, \quad \hat{\boldsymbol{e}}_2 = \frac{\hat{\boldsymbol{e}}_z + \hat{\boldsymbol{e}}_r \, \mathrm{d}a/\mathrm{d}z}{h_2}, \tag{2.8a,b}$$

and

$$h_1 = a, \quad h_2 = \sqrt{1 + \left(\frac{\mathrm{d}a}{\mathrm{d}z}\right)^2}. \tag{2.9a,b}$$

The (outward-pointing) unit normal is therefore given by

$$\hat{\boldsymbol{n}} = \hat{\boldsymbol{e}}_1 \times \hat{\boldsymbol{e}}_2 = \frac{\hat{\boldsymbol{e}}_r - \hat{\boldsymbol{e}}_z \, \mathrm{d}a/\mathrm{d}z}{h_2}, \tag{2.10}$$

see figure 1.

### 2.3. *Deformation*

In principle, the prescription of the deformation from the reference shape $\mathcal{R}$ to the deformed shape $\mathcal{D}$ requires: (i) parametrisation of $\mathcal{R}$ using two variables and (ii) mapping each point on $\mathcal{R}$ to a point in $\mathcal{D}$. Due to the axial symmetry this requires two functions, providing the axial and radial coordinates of the mapped point. Recalling that $\mathcal{R}$ is a sphere of radius $R$, each point on it is parametrised using its azimuthal coordinate $\phi$ and its $z$-coordinate, say $RZ$ ($Z \in [-1, 1]$). The two aforementioned functions, which depend only upon $Z$, are represented by the mappings

$$Z \mapsto z, \quad Z \mapsto r. \tag{2.11a,b}$$

While this procedure may be suitable to numerical solutions, it does not merge with the eventual need to perform an asymptotic analysis in the slender limit. For example, in analysing the flow problem the natural parametrisation is expressed in the context of the deformed shape.

This incompatibility is resolved using a parametrisation in $\mathcal{D}$ in conjunction with the inverse of (2.11*a*). To that end, we denote the preimage of $z$ as $Z(z)$. The function $a(z)$, introduced in the previous subsection, is formally constructed by the composition of $Z(z)$ with (2.11*b*).

It is evident that $Z(z)$ is an odd function that satisfies

$$Z(\pm L) = \pm 1. \tag{2.12}$$

It is tempting to add a condition representing the extrema attained by (2.11*a*) at the two 'ends' of the capsule. In terms of the mapping $Z(z)$, this gives

$$\lim_{|z| \nearrow L} \frac{\sqrt{1 - Z}}{\mathrm{d}Z/\mathrm{d}z} = 0. \tag{2.13}$$

However, given the anticipation of a cusped-end, we avoid that 'spindle-end' condition which only holds for smooth ends. We will provide later the appropriate condition replacing (2.13).

Consider now the deformation of a line element corresponding to infinitesimal increments $(\mathrm{d}\phi, \mathrm{d}z)$. The deformation displaces a point with 'initial' position

$$\boldsymbol{R}(z, \phi) = \hat{\boldsymbol{e}}_r R\sqrt{1 - Z^2(z)} + \hat{\boldsymbol{e}}_z R Z(z) \tag{2.14}$$

to the 'new' position (2.6). Upon differentiating (2.14) we find that

$$\mathrm{d}\boldsymbol{R} = \hat{\boldsymbol{e}}_\phi R\sqrt{1 - Z^2}\,\mathrm{d}\phi + \left(\hat{\boldsymbol{e}}_z - \frac{Z}{\sqrt{1 - Z^2}}\,\hat{\boldsymbol{e}}_r\right) R\frac{\mathrm{d}Z}{\mathrm{d}z}\,\mathrm{d}z. \tag{2.15}$$

Noting that the two basis vectors in $\mathcal{R}$ are (see figure 1)

$$\hat{\boldsymbol{d}}_1 = \hat{\boldsymbol{e}}_\phi, \quad \hat{\boldsymbol{d}}_2 = \hat{\boldsymbol{e}}_z\sqrt{1 - Z^2} - \hat{\boldsymbol{e}}_r Z, \tag{2.16}$$

we find that

$$\mathrm{d}\boldsymbol{R} = \hat{\boldsymbol{d}}_1 R\sqrt{1 - Z^2}\,\mathrm{d}\phi + \hat{\boldsymbol{d}}_2\frac{R\,\mathrm{d}Z/\mathrm{d}z}{\sqrt{1 - Z^2}}\,\mathrm{d}z. \tag{2.17}$$

Since (2.7) gives

$$\mathrm{d}\boldsymbol{r} = \hat{\boldsymbol{e}}_1 h_1\,\mathrm{d}\phi + \hat{\boldsymbol{e}}_2 h_2\,\mathrm{d}z, \tag{2.18}$$

we can read off the principal stretches, namely

$$\lambda_1 = \frac{a}{R\sqrt{1 - Z^2}}, \quad \lambda_2 = \frac{h_2\sqrt{1 - Z^2}}{R\,\mathrm{d}Z/\mathrm{d}z}. \tag{2.19a,b}$$

Note that $\lambda_1$ is the ratio of the deformed radius $a(z)$ to the reference radius at $Z(z)$, see (2.14).

### 2.4. *Flow*

Consider now the flow field in the membrane exterior, where the velocity field is denoted by $\boldsymbol{u}$ and the associated stress tensor by $\boldsymbol{\sigma}$. The flow is governed by the continuity and Stokes equations,

$$\boldsymbol{\nabla}\cdot\boldsymbol{u} = 0, \quad \boldsymbol{\nabla}\cdot\boldsymbol{\sigma} = \boldsymbol{0}. \tag{2.20a,b}$$

At the deformed membrane it satisfies the no-slip condition,

$$\boldsymbol{u} = \boldsymbol{0} \quad \text{for} \quad r = a(z), \tag{2.21}$$

while at large distances it approaches the imposed flow

$$\boldsymbol{u} \sim E\left(z\hat{\boldsymbol{e}}_z - \frac{r}{2}\hat{\boldsymbol{e}}_r\right) \quad \text{as} \quad r^2 + z^2 \to \infty. \tag{2.22}$$

As this is the same problem governing the flow outside a rigid body, the flow is uniquely determined by the shape of the deformed capsule, as provided by the distribution $a(z)$. Since the interior fluid is stationary, the stress there is isotropic, say $-PI$.

For an incompressible flow, the pressure field is generally defined to within an arbitrary additive constant; since the pressure difference across the membrane is physically meaningful, this arbitrariness may only be exploited once, either in the membrane interior or its exterior. With no loss of generality, we set the pressure at infinity to zero, The constant $P$ thereby represents the difference between the uniform interior pressure and the far-field pressure in the exterior region. With that choice, the magnitude of both $\boldsymbol{\sigma}$ and $P$ is proportional to $\mu E$; in particular, $P$ may be interpreted as a 'dynamic' pressure.

Due to axial symmetry, the velocity must be of the form

$$\boldsymbol{u} = \hat{\boldsymbol{e}}_r u + \hat{\boldsymbol{e}}_z w, \tag{2.23}$$

where $u$ and $w$ are functions of $r$ and $z$, but not of $\phi$. Consequently, the Newtonian stress must be of the form

$$\boldsymbol{\sigma} = \hat{\boldsymbol{e}}_r\hat{\boldsymbol{e}}_r\sigma_{rr} + \hat{\boldsymbol{e}}_z\hat{\boldsymbol{e}}_z\sigma_{zz} + (\hat{\boldsymbol{e}}_r\hat{\boldsymbol{e}}_z + \hat{\boldsymbol{e}}_z\hat{\boldsymbol{e}}_r)\sigma_{rz}, \tag{2.24}$$

where $\sigma_{rr}$, $\sigma_{zz}$ and $\sigma_{rz}$ are functions of $r$ and $z$.

### 2.5. *Static equilibrium*

The shape $\mathcal{D}$ of the deformed membrane is governed by the force balance

$$\boldsymbol{\nabla}_s \cdot \mathcal{T}_s + \hat{\boldsymbol{n}} \cdot \boldsymbol{\sigma} + \hat{\boldsymbol{n}} P = \boldsymbol{0} \quad \text{at} \quad r = a(z), \tag{2.25}$$

applying for $-L < z < L$, where $\boldsymbol{\nabla}_s$ is the surface-gradient operator and $\mathcal{T}_s$ the surface stress. By forming the dot product of (2.25) with $\hat{\boldsymbol{e}}_2$ we obtain the meridional balance

$$\hat{\boldsymbol{e}}_2 \cdot (\boldsymbol{\nabla}_s \cdot \mathcal{T}_s) + \hat{\boldsymbol{n}} \cdot \boldsymbol{\sigma} \cdot \hat{\boldsymbol{e}}_2 = 0. \tag{2.26}$$

Similarly, by forming the dot product of (2.25) with $\hat{\boldsymbol{n}}$ we obtain the normal balance

$$\hat{\boldsymbol{n}} \cdot (\boldsymbol{\nabla}_s \cdot \mathcal{T}_s) + \hat{\boldsymbol{n}} \cdot \boldsymbol{\sigma} \cdot \hat{\boldsymbol{n}} + P = 0. \tag{2.27}$$

It is evident from the problem symmetry that the principal directions of the Cauchy tension $\mathcal{T}_s$ are provided by the unit vectors (2.8). We therefore write the Cauchy tension in the form

$$\mathcal{T}_s = \tau_1\hat{\boldsymbol{e}}_1\hat{\boldsymbol{e}}_1 + \tau_2\hat{\boldsymbol{e}}_2\hat{\boldsymbol{e}}_2. \tag{2.28}$$

The component of $\boldsymbol{\nabla}_s \cdot \mathcal{T}_s$ in the meridional direction is

$$\hat{\boldsymbol{e}}_2 \cdot (\boldsymbol{\nabla}_s \cdot \mathcal{T}_s) = \frac{\mathrm{d}\tau_2}{\mathrm{d}s} + \frac{1}{a}\frac{\mathrm{d}a}{\mathrm{d}s}(\tau_2 - \tau_1), \tag{2.29}$$

wherein $s$ is the arclength in the meridional plane, increasing in the direction of $\hat{\boldsymbol{e}}_2$; making use of (2.7*b*) yields

$$\hat{\boldsymbol{e}}_2 \cdot (\boldsymbol{\nabla}_s \cdot \mathcal{T}_s) = \frac{1}{h_2}\left(\frac{\mathrm{d}\tau_2}{\mathrm{d}z} + \frac{\mathrm{d}a}{\mathrm{d}z}\frac{\tau_2 - \tau_1}{a}\right). \tag{2.30}$$

The component of $\boldsymbol{\nabla}_s \cdot \mathcal{T}_s$ in the normal direction is

$$\hat{\boldsymbol{n}} \cdot (\boldsymbol{\nabla}_s \cdot \mathcal{T}_s) = \kappa_1\tau_1 + \kappa_2\tau_2, \tag{2.31}$$

where the principal curvatures are given by

$$\kappa_1 = -\frac{1}{h_2 a}, \quad \kappa_2 = \frac{1}{h_2^3}\frac{\mathrm{d}^2 a}{\mathrm{d}z^2}. \tag{2.32$a$,$b$}$$

Last, making use of (2.8) and (2.10) we find from (2.24) that

$$\hat{\boldsymbol{n}} \cdot \boldsymbol{\sigma} \cdot \hat{\boldsymbol{e}}_2 = \frac{\left[1 - (\mathrm{d}a/\mathrm{d}z)^2\right]\sigma_{rz} + (\mathrm{d}a/\mathrm{d}z)\,(\sigma_{rr} - \sigma_{zz})}{h_2^2}, \tag{2.33$a$}$$

$$\hat{\boldsymbol{n}} \cdot \boldsymbol{\sigma} \cdot \hat{\boldsymbol{n}} = \frac{\sigma_{rr} - 2\,(\mathrm{d}a/\mathrm{d}z)\,\sigma_{rz} + (\mathrm{d}a/\mathrm{d}z)^2\,\sigma_{zz}}{h_2^2}. \tag{2.33$b$}$$

### 2.6. *Axial balance*

Substituting expressions (2.30) and (2.33*a*) into the meridional balance (2.26) yields

$$\frac{\left[1-(\mathrm{d}a/\mathrm{d}z)^2\right]\sigma_{rz}+(\mathrm{d}a/\mathrm{d}z)\,(\sigma_{rr}-\sigma_{zz})}{h_2^2}+\frac{1}{h_2}\left(\frac{\mathrm{d}\tau_2}{\mathrm{d}z}+\frac{\mathrm{d}a}{\mathrm{d}z}\frac{\tau_2-\tau_1}{a}\right)=0. \tag{2.34}$$

Similarly, substituting (2.31) and (2.33*b*) into the normal balance (2.27) yields

$$\frac{\sigma_{rr}-2\,(\mathrm{d}a/\mathrm{d}z)\,\sigma_{rz}+(\mathrm{d}a/\mathrm{d}z)^2\,\sigma_{zz}}{h_2^2}+\kappa_1\tau_1+\kappa_2\tau_2+P=0. \tag{2.35}$$

Note that (2.34)–(2.35) can be combined to get the axial stress balance

$$\frac{\mathrm{d}}{\mathrm{d}z}\left(T-\pi a^2 P\right)=2\pi a\left(\frac{\mathrm{d}a}{\mathrm{d}z}\sigma_{zz}-\sigma_{rz}\right), \tag{2.36}$$

where

$$T=\frac{2\pi a\tau_2}{h_2} \tag{2.37}$$

is the net axial elastic tension.

For a cusped shape we replace (2.13) by the requirement of zero axial tension at the ends of the capsule,

$$T(\pm L)=0. \tag{2.38}$$

This condition eliminates the possibility of point singularities at the tips, thus selecting the least-singular solution (Van Dyke 1964). Note that (2.38) is trivially satisfied for rounded ends, where $a\to 0$ and $|h_2|\to\infty$ (recall (2.7*b*)).

### 2.7. *Elasticity*

The evaluation of the Cauchy elastic tension $\mathcal{T}_s$ requires consideration of the elastic deformation. The principal values of $\mathcal{T}_s$, $\tau_{1,2}$, are functions of the principal extensional stretches (4.8). Dimensional arguments for the state of stretch imply that

$$\tau_{1,2}/G=\text{functions of }\lambda_1,\,\lambda_2,\,K/G. \tag{2.39}$$

Hereafter, we assume the Skalak model (Skalak *et al.* 1973), where

$$\frac{\tau_1}{G}=\frac{\lambda_1\left(\lambda_1^2-1\right)}{\lambda_2}+C\lambda_1\lambda_2\left(\lambda_1^2\lambda_2^2-1\right),\quad \frac{\tau_2}{G}=\frac{\lambda_2\left(\lambda_2^2-1\right)}{\lambda_1}+C\lambda_1\lambda_2\left(\lambda_1^2\lambda_2^2-1\right). \tag{2.40$a$,$b$}$$

The dimensionless parameter,

$$C=\frac{K/G-1}{2}, \tag{2.41}$$

is associated with resistance to area dilatation (Barthès-Biesel *et al.* 2002).

## 3. Strong flow: scaling

Henceforth, we focus upon the case of strong flow,

$$Ca\gg 1. \tag{3.1}$$

In this asymptotic limit, we expect $\epsilon$ to be small,

$$\epsilon \ll 1. \tag{3.2}$$

Our interest is in the dependence of $\epsilon$ and $L/R$ upon $Ca$ in the limit (3.1). It is preferable to temporarily adopt a mathematically equivalent approach where $\epsilon$ and $L$ are considered as known, the former satisfying (3.2). The capillary number $Ca$ and the reference radius $R$ are then effectively considered as functions of $\epsilon$ and $L$.

Prior to carrying an approximate scheme in the limit (3.2), we perform a scaling analysis. In what follows, we employ $\simeq$ to imply 'of order'. In that context, the key estimates are

$$z \simeq L, \quad a \simeq \epsilon L. \tag{3.3a,b}$$

It is evident from (2.5) and (3.3) that

$$R \simeq L\epsilon^{2/3}. \tag{3.4}$$

We consider first the elastic stresses. Formulae (2.19) for the principal stretches in conjunction with (3.3) imply that $\lambda_1 \simeq \epsilon L/R$ and $\lambda_2 \simeq L/R$. Using (3.4) we find

$$\lambda_1 \simeq \epsilon^{1/3}, \quad \lambda_2 \simeq \epsilon^{-2/3} \tag{3.5a,b}$$

and, consequently, $\lambda_1\lambda_2 \simeq \epsilon^{-1/3}$. Substitution into (2.40) gives

$$\tau_1 \simeq G\epsilon^{-1}, \quad \tau_2 \simeq G\epsilon^{-7/3}, \tag{3.6a,b}$$

so that

$$\tau_2 \gg \tau_1, \tag{3.7}$$

as would be expected under strong elongation.

It is evident from (2.32) that

$$\kappa_1 \simeq \frac{1}{\epsilon L}, \quad \kappa_2 \simeq \frac{\epsilon}{L}, \tag{3.8a,b}$$

whereby

$$\kappa_1\tau_1 \simeq GL^{-1}\epsilon^{-2}, \quad \kappa_2\tau_2 \simeq GL^{-1}\epsilon^{-4/3}, \tag{3.9a,b}$$

so, despite (3.7),

$$\kappa_1\tau_1 \gg \kappa_2\tau_2. \tag{3.10}$$

Consider now the divergence of $\mathcal{T}_s$. It is evident from (2.30) and (3.7) that

$$\hat{\boldsymbol{e}}_2 \cdot (\boldsymbol{\nabla}_s \cdot \mathcal{T}_s) \simeq \tau_2/L. \tag{3.11}$$

It also follows from (2.31) and (3.10) that

$$\hat{\boldsymbol{n}} \cdot (\boldsymbol{\nabla}_s \cdot \mathcal{T}_s) \simeq \kappa_1\tau_1. \tag{3.12}$$

Substituting (3.6) and (3.9*a*) into (3.11) and (3.12) yields

$$\hat{\boldsymbol{e}}_2 \cdot (\boldsymbol{\nabla}_s \cdot \mathcal{T}_s) \simeq GL^{-1}\epsilon^{-7/3}, \quad \hat{\boldsymbol{n}} \cdot (\boldsymbol{\nabla}_s \cdot \mathcal{T}_s) \simeq GL^{-1}\epsilon^{-2}. \tag{3.13a,b}$$

With the azimuthal component subdominant, the scaling relation between $Ca$ and $\epsilon$ is determined by the meridional balance (2.26). (In that sense, the present problem is fundamentally different from the classical problem of a deforming bubble.) To determine

that relation we need to estimate the hydrodynamic stress. We first recall that $\boldsymbol{\sigma}$ scales as $\mu E$. For small $\epsilon$ the shear-stress magnitude is amplified by $1/\epsilon$, so

$$\hat{\boldsymbol{n}} \cdot \boldsymbol{\sigma} \cdot \hat{\boldsymbol{e}}_2 \simeq \frac{\mu E}{\epsilon}. \tag{3.14}$$

Making use of (3.13*a*) and (3.14), the meridional balance (2.26) gives

$$\frac{G}{L\epsilon^{7/3}} \simeq \frac{\mu E}{\epsilon}. \tag{3.15}$$

Making use of (2.1) and (3.4) we obtain the requisite scaling

$$Ca \simeq \epsilon^{-2/3}. \tag{3.16}$$

For future reference we note from (3.13) that the ratio of $\hat{\boldsymbol{n}} \cdot (\boldsymbol{\nabla}_s \cdot \mathcal{T}_s)$ to $\hat{\boldsymbol{e}}_2 \cdot (\boldsymbol{\nabla}_s \cdot \mathcal{T}_s)$ is $\simeq \epsilon^{1/3}$.

## 4. Analysis

We now go beyond scaling, carrying out a systematic approximation scheme. We retain our 'inverted' approach where $\epsilon$ and $L$ are considered as given.

### 4.1. *Dimensionless variables*

At this stage we find it useful to introduce the dimensionless axial coordinate (recall (3.3*a*)),

$$\zeta = z/L. \tag{4.1}$$

This induces the definition of the dimensionless mapping $\Psi(\zeta)$,

$$Z(z) = \Psi(\zeta), \tag{4.2}$$

and the dimensionless shape function $\Phi(\zeta)$ (recall (3.3*b*))

$$a(z) = \epsilon L \Phi(\zeta). \tag{4.3}$$

We note that $\Phi(\zeta)$ is an even function while $\Psi(\zeta)$ is an odd function.

In dimensionless form, conditions (2.3) and (2.12) are

$$\Phi(\pm 1) = 0, \quad \Psi(\pm 1) = \pm 1, \tag{4.4a,b}$$

while the waist condition (2.4) becomes

$$\Phi(0) = 1. \tag{4.5}$$

Following (3.4) we define

$$R = L\epsilon^{2/3}\chi, \tag{4.6}$$

The volume constraint (2.5) thus becomes

$$\int_{-1}^{1} \Phi^2(\zeta)\,\mathrm{d}\zeta = \frac{4\chi^3}{3}. \tag{4.7}$$

The principal stretches (2.19) become, in terms of $\Phi$ and $\Psi$,

$$\lambda_1 = \frac{\epsilon L}{R}\frac{\Phi}{\sqrt{1-\Psi^2}}, \quad \lambda_2 = \frac{L}{R}\frac{h_2\sqrt{1-\Psi^2}}{\mathrm{d}\Psi/\mathrm{d}\zeta}. \tag{4.8a,b}$$

### 4.2. *Approximations for elastic stresses*

We proceed with a leading-order analysis. In what follows, the symbol '$\sim$' implies 'asymptotic to,' with the understanding that the associated error is 'algebraically small' (i.e. asymptotically smaller than some positive power of $\epsilon$).

We begin with the geometric quantities. Using (4.1) and (4.3), we see that the scale factors introduced in (2.9) are given by

$$h_1 = \epsilon L \Phi, \quad h_2 \sim 1, \tag{4.9a,b}$$

while the principal curvatures (2.32) become

$$\kappa_1 \sim -\frac{1}{\epsilon L \Phi}, \quad \kappa_2 \sim \frac{\epsilon \Phi}{L}. \tag{4.10a,b}$$

Upon making use of (4.6) and (4.9*b*), the principal stretches (4.8) simplify to

$$\lambda_1 = \frac{\epsilon^{1/3}}{\chi} \frac{\Phi}{\sqrt{1-\Psi^2}}, \quad \lambda_2 \sim \frac{1}{\epsilon^{2/3}\chi} \frac{\sqrt{1-\Psi^2}}{\mathrm{d}\Psi/\mathrm{d}\zeta}. \tag{4.11a,b}$$

Consider now the elastic constitutive relations (2.40). Making use of (3.5), we find that they are approximated by

$$\frac{\tau_1}{G} \sim C\lambda_1^3\lambda_2^3, \quad \frac{\tau_2}{G} \sim \frac{\lambda_2^3}{\lambda_1}. \tag{4.12a,b}$$

Substituting (4.11) thus gives

$$\frac{\tau_1}{G} \sim \frac{C}{\chi^6\epsilon} \frac{\Phi^3}{(\mathrm{d}\Psi/\mathrm{d}\zeta)^3}, \quad \frac{\tau_2}{G} \sim \frac{1}{\chi^2\epsilon^{7/3}} \frac{\left(1-\Psi^2\right)^2}{\Phi\,(\mathrm{d}\Psi/\mathrm{d}\zeta)^3}. \tag{4.13a,b}$$

Consider now the divergence of $\mathcal{T}_s$. Making use of (2.30) and noting that $\tau_2 \gg \tau_1$ we obtain the meridional component

$$\hat{\boldsymbol{e}}_2 \cdot (\boldsymbol{\nabla}_s \cdot \mathcal{T}_s) \sim \frac{1}{a}\frac{\mathrm{d}}{\mathrm{d}z}(a\tau_2). \tag{4.14}$$

Upon substituting (4.1)–(4.3) and (4.13*b*) we obtain

$$\frac{\hat{\boldsymbol{e}}_2 \cdot (\boldsymbol{\nabla}_s \cdot \mathcal{T}_s)}{G/L} \sim \frac{1}{\chi^2\epsilon^{7/3}} \frac{1}{\Phi} \frac{\mathrm{d}}{\mathrm{d}\zeta}\left[\frac{\left(1-\Psi^2\right)^2}{(\mathrm{d}\Psi/\mathrm{d}\zeta)^3}\right]. \tag{4.15}$$

Making use of (2.31) and (3.10) we obtain $\hat{\boldsymbol{n}} \cdot (\boldsymbol{\nabla}_s \cdot \mathcal{T}_s) \sim \kappa_1\tau_1$. Substitution of (4.10*a*) and (4.13*a*) gives

$$\frac{\hat{\boldsymbol{n}} \cdot (\boldsymbol{\nabla}_s \cdot \mathcal{T}_s)}{G/L} \sim -\frac{C}{\chi^6\epsilon^2} \frac{\Phi^2}{(\mathrm{d}\Psi/\mathrm{d}\zeta)^3}. \tag{4.16}$$

The negative sign implies a surface-tension-like 'inward' contribution to the normal force balance.

### 4.3. *Flow*

In the limit (3.2), the flow coincides with that about a slender rigid body (Batchelor 1970; Cox 1970; Tillett 1970). In analysing flows about rigid bodies, interest typically lies in the hydrodynamic force acting on the body (or, by extension, in the hydrodynamic couple or the net stresslet strength). For these quantities, it suffices to determine the distribution of Stokeslets that represent the body.

In the present problem, however, we need the actual shear stress at the boundary of the body. For that reason, it is desirable to employ an analysis in the spirit of matched asymptotic expansions, where the Stokeslet distribution represents an approximation on the 'long' scale of body length which is supplemented by a comparable approximation on the 'short' cross-sectional scale $\epsilon$.

Given our desire for an algebraically accurate approximation, we prefer to employ the analysis of Keller & Rubinow (1976), which for the most part avoids an expansion in inverse powers of $\ln\epsilon$. Adapting their analysis to the present notation, the long-scale flow is written as a superposition of the ambient flow (2.22) and a collection of Stokeslets (of strength $\mu EL\mathcal{F}$ per unit length) along the symmetry axis,

$$\frac{\boldsymbol{u}}{EL}\sim\zeta\hat{\boldsymbol{e}}_z-\frac{\rho}{2}\hat{\boldsymbol{e}}_r+\frac{1}{8\pi}\int_{-1}^{1}\mathcal{F}(\xi)\left\{\frac{\hat{\boldsymbol{e}}_z}{\left[\rho^2+(\zeta-\xi)^2\right]^{1/2}}+(\zeta-\xi)\frac{\hat{\boldsymbol{e}}_r\rho+\hat{\boldsymbol{e}}_z(\zeta-\xi)}{\left[\rho^2+(\zeta-\xi)^2\right]^{3/2}}\right\}\mathrm{d}\xi, \tag{4.17}$$

wherein (cf. (4.1))

$$\rho=r/L. \tag{4.18}$$

On the cross-sectional scale, where $\rho=O(\epsilon)$, the flow is primarily in the axial direction. Thus, making use of the form (2.23), $w/EL=O(1)$ while $u/EL$ is $O(\epsilon)$. In particular, imposing the no slip condition at $\rho/\epsilon=\Phi$ and compatibility with (4.17) yields (see equations (1), (2) and (9) in Keller & Rubinow (1976))

$$\frac{w}{EL}\sim-\frac{\mathcal{F}(\zeta)}{2\pi}\ln\frac{\rho}{\epsilon\Phi(\zeta)}. \tag{4.19}$$

The integral equation governing the Stokelet distribution $\mathcal{F}(\zeta)$ was determined by Keller & Rubinow (1976) via matching between the long-scale and short-scale solutions (see equation (12) in Keller & Rubinow (1976)). Adapting to the present notation, this equation reads

$$4\pi\zeta+[\ln(1-\zeta^2)-1]\mathcal{F}(\zeta)+\int_{-1}^{1}\frac{\mathcal{F}(\xi)-\mathcal{F}(\zeta)}{|\xi-\zeta|}\,\mathrm{d}\xi=2\mathcal{F}(\zeta)\ln\frac{\epsilon\Phi(\zeta)}{2}. \tag{4.20}$$

Consistently with our approach (and, more generally, with established asymptotic practices (Fraenkel 1969)), we retain terms that are logarithmically small in $\epsilon$ while neglecting algebraically small corrections.

We can now calculate the hydrodynamic shear stress in terms of $\mathcal{F}$. It is evident that on the cross-sectional scale $\sigma_{rz}\sim\mu\,\partial w/\partial r$. Substituting (4.18) and (4.19) we obtain the $O(\epsilon^{-1})$ stress (cf. (3.14)),

$$\sigma_{rz}/\mu E\sim-\frac{\mathcal{F}(\zeta)}{2\pi\epsilon\Phi(\zeta)}\quad\text{at}\quad\rho=\epsilon\Phi(\zeta). \tag{4.21}$$

It is readily verified that both $\sigma_{rr}/\mu E$ and $\sigma_{zz}/\mu E$ are $O(1)$ on the cross-sectional scale. From (2.33) we then conclude that

$$\frac{\hat{\boldsymbol{n}}\cdot\boldsymbol{\sigma}\cdot\hat{\boldsymbol{e}}_2}{\mu E}\sim-\frac{\mathcal{F}(\zeta)}{2\pi\epsilon\Phi(\zeta)},\qquad\frac{\hat{\boldsymbol{n}}\cdot\boldsymbol{\sigma}\cdot\hat{\boldsymbol{n}}}{\mu E}=O(1). \tag{4.22a,b}$$

### 4.4. *Dominant balances*

Requiring that the two terms in meridional equilibrium (2.26) balance, we find using (4.15) and (4.22*a*) that

$$\frac{G/L}{\chi^2\epsilon^{7/3}}\frac{\mathrm{d}}{\mathrm{d}\zeta}\left[\frac{\left(1-\Psi^2\right)^2}{\left(\mathrm{d}\Psi/\mathrm{d}\zeta\right)^3}\right]\sim\frac{\mu E\mathcal{F}}{2\pi\epsilon} \tag{4.23}$$

Making use of (2.1) and (4.6) we obtain

$$2\pi\frac{\mathrm{d}}{\mathrm{d}\zeta}\left[\frac{\left(1-\Psi^2\right)^2}{\left(\mathrm{d}\Psi/\mathrm{d}\zeta\right)^3}\right]\sim Ca\;\chi\epsilon^{2/3}\mathcal{F}. \tag{4.24}$$

Thus, $Ca$ scales as $\epsilon^{-2/3}$, as already anticipated in (3.16). Defining the rescaled capillary number

$$\widetilde{Ca}=Ca\;\chi\epsilon^{2/3} \tag{4.25}$$

we obtain

$$\frac{\mathrm{d}\Omega}{\mathrm{d}\zeta}\sim\widetilde{Ca}\,\mathcal{F}(\zeta), \tag{4.26}$$

wherein

$$\Omega(\zeta)=2\pi\,\frac{\left(1-\Psi^2\right)^2}{\left(\mathrm{d}\Psi/\mathrm{d}\zeta\right)^3} \tag{4.27}$$

is a (leading-order) dimensionless version of the axial tension (2.37),

$$\Omega=\epsilon^2\chi^3\frac{T}{GR}. \tag{4.28}$$

Consider now the normal balance (2.27). It follows from (2.1), (4.6), (4.16) and (4.22*b*) that the ratio of $\hat{\boldsymbol{n}}\cdot\boldsymbol{\sigma}\cdot\hat{\boldsymbol{n}}$ to $\hat{\boldsymbol{n}}\cdot(\boldsymbol{\nabla}_s\cdot\mathcal{T}_s)$ is of order $Ca\,\epsilon^{4/3}$, or, using (3.16), of order $\epsilon^{2/3}$. This was to be expected, we already saw from the scaling estimate (3.13) that the normal component of $\boldsymbol{\nabla}_s\cdot\mathcal{T}_s$ is $O(\epsilon^{1/3})$ relative to meridional component. The hydrodynamic considerations, on the other hand, have revealed that the ratio of the normal Newtonian stress to the shear Newtonian stress is of order $\epsilon$. It follows that the hydrodynamic traction does not participate at the dominant balance of (2.27), which must therefore involve the elastic force (4.16) and the core pressure. Defining the dimensionless pressure

$$\Pi=\frac{P}{\mu E}, \tag{4.29}$$

we therefore obtain

$$\frac{G}{L}\frac{C}{\chi^6\epsilon^2}\frac{\Phi^2}{\left(\mathrm{d}\Psi/\mathrm{d}\zeta\right)^3}\sim\mu E\Pi. \tag{4.30}$$

Making use of (2.1), (4.6) and (4.25) yields the dimensionless balance

$$\frac{\Phi^2}{\left(\mathrm{d}\Psi/\mathrm{d}\zeta\right)^3}\sim\epsilon^{2/3}\frac{\chi^4\widetilde{Ca}}{C}\Pi. \tag{4.31}$$

It follows that $\Pi$ scales as $\epsilon^{-2/3}$ – namely as the capillary number. Defining the rescaled pressure,

$$\widetilde{\Pi} = \epsilon^{2/3} \frac{\chi^4 \widetilde{Ca}}{C} \Pi, \tag{4.32}$$

we find that (4.31) is simplified to

$$\Phi = \widetilde{\Pi}^{1/2} \left( \frac{\mathrm{d}\Psi}{\mathrm{d}\zeta} \right)^{3/2}, \tag{4.33}$$

where we used the fact that both $\Phi$ and $\mathrm{d}\Psi/\mathrm{d}\zeta$ are non-negative.

## 5. Reduced problem

We now summarise the reduced problem governing the mapping $\Psi$ and the tension $\Omega$ introduced in (4.27). Relation (4.27) is rewritten as a first-order differential equation,

$$\frac{\mathrm{d}\Psi}{\mathrm{d}\zeta} = (2\pi)^{1/3} \frac{\left(1-\Psi^2\right)^{2/3}}{\Omega^{1/3}}. \tag{5.1}$$

The shape is obtained from (4.33) and (5.1)

$$\Phi = (2\pi\widetilde{\Pi})^{1/2} \frac{1-\Psi^2}{\Omega^{1/2}}. \tag{5.2}$$

Substituting (4.26) and (5.2) into (4.20), we obtain

$$4\pi \widetilde{Ca}\, \zeta + \left[\ln(1-\zeta^2) - 1\right] \Omega'(\zeta) + \int_{-1}^{1} \frac{\Omega'(\xi) - \Omega'(\zeta)}{|\xi - \zeta|}\, \mathrm{d}\xi = \Omega'(\zeta) \ln \frac{\epsilon^2 \pi \widetilde{\Pi} (1-\Psi^2)}{2\Omega}, \tag{5.3}$$

where the prime denotes differentiation. The deformation problem is therefore governed by the set (5.1) and (5.3).

Since $\Psi(\zeta)$ is an odd function, $\Omega(\zeta)$ must be even: see (4.27). We therefore solve only for $\zeta > 0$, replacing (5.3) by

$$\begin{aligned} &\Omega'(\zeta) \ln \frac{\epsilon^2 \pi \widetilde{\Pi} (1-\Psi^2)}{2\Omega} - 4\pi \widetilde{Ca}\, \zeta \\ &\quad = \left[\ln(1-\zeta^2) - 1\right] \Omega'(\zeta) + \int_0^1 \frac{\Omega'(\xi) - \Omega'(\zeta)}{|\xi - \zeta|}\, \mathrm{d}\xi - \int_0^1 \frac{\Omega'(\xi) + \Omega'(\zeta)}{|\xi + \zeta|}\, \mathrm{d}\xi, \end{aligned} \tag{5.4}$$

and adding the symmetry conditions

$$\Omega'(0) = 0, \quad \Psi(0) = 0. \tag{5.5a,b}$$

These are supplemented by the end condition,

$$\Psi(1) = 1, \tag{5.6}$$

which follows from (4.4) and (5.2); the waist condition

$$\Omega(0) = 2\pi\widetilde{\Pi}, \tag{5.7}$$

which follows from (4.5) and (5.2); and the tip condition,

$$\Omega(1) = 0, \tag{5.8}$$

which constitutes the dimensionless version of (2.38).

We note that (5.5*a*) is trivially satisfied by (5.4). Thus, (5.1) and (5.4) together with the four conditions (5.5*b*)–(5.8) presumably provide a closed system for $\Omega(\zeta)$ and $\Psi(\zeta)$, in which the dimensionless parameters $\widetilde{Ca}$ and $\widetilde{\Pi}$ are determined as part of the solution. Conveniently, the above problem is independent of $\chi$. Once the problem is solved, $\chi$ may be determined from the relation

$$\pi\widetilde{\Pi}\int_0^1 \frac{(1-\Psi^2)^2}{\Omega}\,\mathrm{d}\zeta = \frac{\chi^3}{3}, \tag{5.9}$$

which follows from (4.7) in conjunction with (5.2). The dimensionless capsule length and capillary number corresponding to the chosen value of $\epsilon$ are then recovered from (4.6) and (4.25), respectively.

We note that the reduced problem is independent of $C$. Once the problem is solved and $\widetilde{\Pi}$ is calculated, the value of $C$ affects the core pressure $\Pi$, see (4.32). Otherwise, $C$ does not affect the capsule shape at the present leading-order approximation scheme.

## 6. Logarithmic approximation

Let us derive a 'logarithmically accurate' approximation by considering $\ln(2/\epsilon^2)$ as being asymptotically large. The associated leading-order balance in (5.4) then takes place between the two terms on the left-hand side. We can therefore make the leading-order approximation

$$\frac{\mathrm{d}\Omega}{\mathrm{d}\zeta} \approx -\frac{4\pi\widetilde{Ca}\,\zeta}{\ln\left(2/\epsilon^2\right)}, \tag{6.1}$$

where the symbol '$\approx$' is used to represent the 'logarithmic' approximation.

We can immediately integrate (6.1) and apply the tip condition (5.8) to get the leading-order tension

$$\Omega(\zeta) \approx \frac{2\pi\widetilde{Ca}\,\left(1-\zeta^2\right)}{\ln\left(2/\epsilon^2\right)}, \tag{6.2}$$

whereby condition (5.7) yields

$$\widetilde{\Pi} \approx \frac{\widetilde{Ca}}{\ln\left(2/\epsilon^2\right)}. \tag{6.3}$$

From (5.1) we then obtain the separable equation

$$\frac{\widetilde{\Pi}^{1/3}}{\left(1-\Psi^2\right)^{2/3}}\frac{\mathrm{d}\Psi}{\mathrm{d}\zeta} \approx \frac{1}{\left(1-\zeta^2\right)^{1/3}}, \tag{6.4}$$

which may be immediately integrated to give

$$\widetilde{\Pi}^{1/3}\Psi\,{}_2F_1\left(\frac{1}{2},\frac{2}{3},\frac{3}{2};\Psi^2\right) \approx \zeta\,{}_2F_1\left(\frac{1}{3},\frac{1}{2},\frac{3}{2};\zeta^2\right), \tag{6.5}$$

in which ${}_2F_1$ is a hypergeometric function, and the integration constant vanishes because of condition (5.5*b*).

Application of (5.6) gives

$$\widetilde{\Pi} \approx \left[\frac{{}_2F_1\,(1/3,\,1/2,\,3/2;\,1)}{{}_2F_1\,(1/2,\,2/3,\,3/2;\,1)}\right]^3 = \frac{\pi^{3/2}\left[\Gamma\,(5/6)\right]^3}{54\left[\Gamma\,(7/6)\right]^6}. \tag{6.6}$$

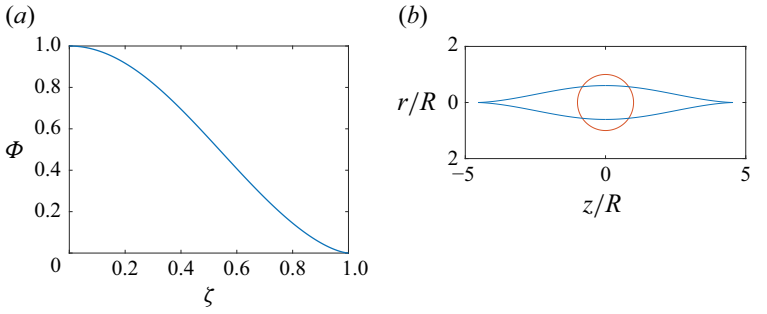


Figure 2. Logarithmic approximation: *(a)* universal shape, $\Phi$ versus $\zeta$; (*b*) physical shape in the $(r/R, z/R)$ coordinates for $Ca = 5$.

By expanding (6.5) near $\zeta = 1$ and $\Psi = 1$ we obtain, using (6.6),

$$\Psi(\zeta) \sim 1 - \frac{\pi^{3/2}\left[\Gamma(7/6)\right]^3}{2\left[\Gamma(5/6)\right]^6}(1-\zeta)^2 \quad \text{as} \quad \zeta \nearrow 1. \tag{6.7}$$

Given (6.6), the implicit relation (6.5) provides $\Psi$ as a function of $\zeta$, independent of $\epsilon$. Substituting (6.2) and (6.3) into (5.2) yields the shape

$$\Phi = \frac{1-\Psi^2}{(1-\zeta^2)^{1/2}}. \tag{6.8}$$

Note that (6.7) and (6.8) implies that $\Phi$ behaves like $(1-\zeta)^{3/2}$ as $\zeta \nearrow 1$, consistently with the assumption of a cusp. The universal shape, as obtained from substitution of (6.5) and (6.6) into (6.8), is shown in figure 2(*a*).

The volume constraint (5.9) reads here

$$\int_0^1 \frac{\left(1-\Psi^2\right)^2}{1-\zeta^2}\,\mathrm{d}\zeta = \frac{2\chi^3}{3}, \tag{6.9}$$

independently of $\epsilon$. Evaluation using the universal function provided by (6.5) and (6.6) yields

$$\chi = 0.8448\ldots. \tag{6.10}$$

The capsule length is obtained from (4.6) as

$$L/R \approx 1.1837\epsilon^{-2/3}, \tag{6.11}$$

while evaluation of (6.6) gives

$$\widetilde{\Pi} = 0.2326\ldots. \tag{6.12}$$

The capillary number is obtained from (4.25), which upon using (6.3), (6.10) and (6.12) gives

$$Ca \approx 0.2753\,\epsilon^{-2/3}\ln\frac{2}{\epsilon^2} \tag{6.13}$$

With the universal shape $\Phi(\zeta)$ available, we may employ (4.1), (4.3) and (6.11) to plot the 'physical shape' of the capsule on the length scale $R$ for a given capillary number, with the slenderness $\epsilon$ determined from (6.13). In figure 2(b) we plot that physical shape for $Ca = 5$. The reference spherical shape is also shown.

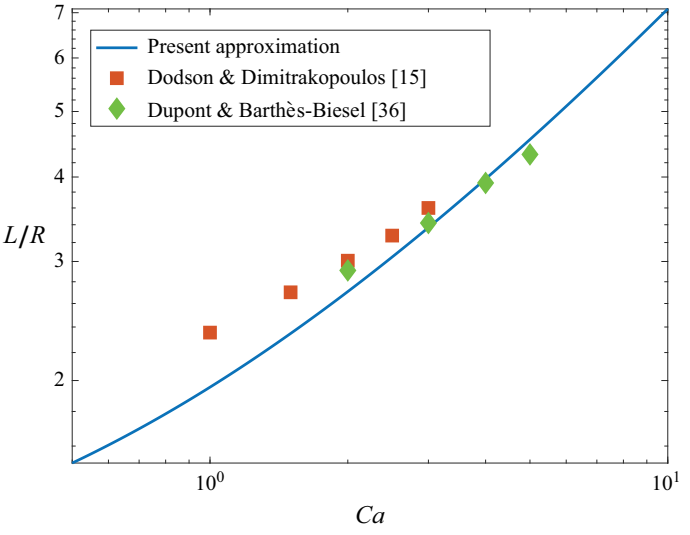


Figure 3. Normalised capsule length $L/R$ as a function of $Ca$: solid, logarithmic approximation, (6.11) and (6.13); squares, data set from Dodson III & Dimitrakopoulos (2009); diamonds, data set from Dupont & Barthés-Biesel (2024).

In comparing our approximation with the existing literature we employ two sets of data points, both obtained for the Skalak law (2.40) with $C = 1$. The first is obtained from the numerical simulations of Dodson III & Dimitrakopoulos (2009). While these authors consider planar hyperbolic flow, it is plausible that these results are quantitatively similar to those of uniaxial flow; indeed, Hinch & Acrivos (1979) analysed bubble deformation in planar flow by viewing it as a perturbation of the axisymmetric case. By interpolating from figure 16 in Dodson III & Dimitrakopoulos (2009), we obtained values of $L/R$ for the $Ca$ values 1, 1.5, 2 and 2.5; in addition, Dodson III & Dimitrakopoulos (2009) cite the value $L/R = 3.6$ for $Ca = 3$. The second set was kindly provided by Dupont & Barthés-Biesel (2024) who recently performed numerical simulations of the present problem. We used their results for the $Ca$ values 2, 3, 4 and 5. Note that the physical shape in figure 2(*b*) has been portrayed for their maximal value of $Ca$.

The comparison is shown in figure 3 where the theoretical approximation for $L/R$ as a function of $Ca$ is obtained from (6.11) and (6.13). Given the crude nature of the logarithmic approximation and the rather modest $Ca$-values which have been employed in the simulations, the agreement is gratifying.

## 7. Neo-Hookean membranes

The preceding analysis was carried out for an elastic membrane governed by the Skalak constitutive description. In principle, it can be carried out for other elastic models, provided the membrane reaches a steady state under large deformation.

In fact, the very possibility of steady state can be inferred from a scaling analysis akin to that carried out in § 3. As an illustration, consider the neo-Hookean model (Barthès-Biesel *et al.* 2002) where (2.40) is replaced by

$$\frac{\tau_1}{G} = \frac{\lambda_1}{\lambda_2} - \frac{1}{\lambda_1^3\lambda_2^3}, \quad \frac{\tau_2}{G} = \frac{\lambda_2}{\lambda_1} - \frac{1}{\lambda_1^3\lambda_2^3}. \tag{7.1a,b}$$

Making use of (3.5), we find that the stress estimates (3.6) are replaced by

$$\tau_1 \simeq G\epsilon, \quad \tau_2 \simeq G\epsilon^{-1}, \tag{7.2a,b}$$

while the estimates (3.9) are replaced by

$$\kappa_1\tau_1, \kappa_2\tau_2 \simeq GL^{-1}. \tag{7.3}$$

Since (3.11) still holds, we find using (7.2*b*) that (3.13*a*) is replaced by

$$\hat{\boldsymbol{e}}_2 \cdot (\boldsymbol{\nabla}_s \cdot \mathcal{T}_s) \simeq GL^{-1}\epsilon^{-1}. \tag{7.4}$$

Also, from (2.31) and (7.3) it follows that (3.13*b*) is replaced by

$$\hat{\boldsymbol{n}} \cdot (\boldsymbol{\nabla}_s \cdot \mathcal{T}_s) \simeq GL^{-1}. \tag{7.5}$$

Thus, just like in the Skalak model, $\hat{\boldsymbol{e}}_2 \cdot (\boldsymbol{\nabla}_s \cdot \mathcal{T}_s) \gg \hat{\boldsymbol{n}} \cdot (\boldsymbol{\nabla}_s \cdot \mathcal{T}_s)$. Balancing (7.4) with (3.14), the meridional balance (2.26) gives (cf. (3.15))

$$\frac{G}{L\epsilon} \simeq \frac{\mu E}{\epsilon}. \tag{7.6}$$

Making use of (2.1) and (3.4) we obtain the scaling

$$Ca \simeq \epsilon^{2/3}, \tag{7.7}$$

which contradicts (3.2). This indicates the impossibility of a steady slender shape. Our conclusion is compatible with the numerical simulations of Barthès-Biesel *et al.* (2002), who observed that a neo-Hookean capsule stretches indefinitely in an elongational flow.

The key to a possible slender limit is the need for the elastic stresses to increase sufficiently fast with diminishing $\epsilon$ so as to overcome the viscous stress that grows as $\epsilon^{-1}$, see (3.14). For a given reference radius $R$, the meridional components of $\boldsymbol{\nabla}_s \cdot \mathcal{T}_s$ increases with diminishing $\epsilon$ in both the Skalak and neo-Hookean models, but at quite different rates. In the Skalak model, it scales as $\epsilon^{-5/3}$ (recall (3.4) and (3.13*a*)), thus giving rise to the scaling relation (3.16) which is compatible with (3.2). In the neo-Hookean model, it scales as $\epsilon^{-1/3}$ (see (3.4) and (7.4)); since the modest growth rate with diminishing $\epsilon$ does not overcome that in (3.14), the resulting scaling (7.7) is incompatible with the slenderness assumption (3.2).

The scaling analyses in the present paper thus provide a rigorous manner to discriminate between strain-softening and strain-hardening models.

## 8. Discussion

Using slender-body approximations, we derived a reduced model governing the deformation of an elastic capsule in a strong hyperbolic straining flow. The asymptotic description consists of the integral equation (5.3) and the first-order differential equation (5.1). The former may be considered as an equation governing the tension $\Omega$; the latter as an equation governing the mapping $\Psi$ relating the reference and present membrane geometries. Interpreting these equations as two first-order ordinary differential equations, their solution introduces two integration constants. Since these equations also involve the two unknown parameters $\widetilde{Ca}$ and $\widetilde{\Pi}$, four auxiliary conditions are required. These are provided by (5.5*b*)–(5.8). Of the original six conditions, (5.5*a*) is trivially satisfied while the two conditions $\Phi(1) = 0$ and $\Psi(1) = 1$ are not independent because of (5.2).

It is important to emphasise, however, that all the original six conditions are required when $\epsilon$ is not small. This is compatible with the effective reduction of order that takes place in the limit $\epsilon \to 0$. Indeed, with $\kappa_2$ algebraically small compared with $\kappa_1$

(recall (4.10)), the second derivative of $\Phi$ does not appear in the reduced problem. The reduction of order suggests that the scale disparity (3.8) should fail in a neighbourhood of the capsule tips, where the highest-derivative term in $\kappa_2$ must come into play. For the case of an inviscid bubble, Buckmaster (1972) speculates that slender-body theory breaks down in a region near the tips that is exponentially small in $\epsilon$, and the same may be true in our case. It is also possible that our approximation becomes non-uniform near the equator, where the assumption of strong flow breaks down (Acrivos & Lo 1978).

The end goal of our contribution has been the calculation of the capsule deformation, and in particular its lumped description by the scalar quantities $\epsilon$ and $L/R$. Our analysis has additionally provided asymptotic information on the elastic stress system created by the imposed elongation. We here wish to address two aspects of that system, both associated with the parameter $C$, as given by (2.41).

The first has to do with the possibility of buckling. If the azimuthal stress is compressive ($\tau_1 < 0$) the axisymmetric shape may become unstable, resulting in a cross-sectional buckling. This symmetry breaking cannot be captured by (numerical or asymptotic) models that are predicated upon axial symmetry. In the present asymptotic description, $\tau_1$ is given by (4.13*a*), representing a situation where the first term on the right-hand side of (2.40*a*) is subdominant. While $C$ is strictly $> -1/2$, it is universally considered non-negative in the literature. (For example, Barthès-Biesel *et al.* (2002) considered the $C$ values 0, 1, 10 and 100.) With (4.13*a*) being non-negative for $C \geqslant 0$, our axisymmetric profiles are stable. This observation agrees with the (fully three-dimensional) numerical simulations of Dupont & Barthés-Biesel (2024), carried out for $C = 1$, which predict buckling only for small values of $Ca$.

The second observation has to do with the limit of large $C$. The terms proportional to $C$ in (2.40) are associated with resistance to area dilatation. Indeed, nearly inextensible membranes (e.g. lipid bilayers) have been analysed in the literature assuming $C \gg 1$ (Skalak *et al.* 1973). It may appear as though the limit $C \gg 1$ in the present description merely results in a core pressure that is much larger than $\epsilon^{-2/3}$ (recall (4.32)). However, the underlying approximation (4.12*b*) breaks down for $C = O(\epsilon^{-4/3})$, when the second term on the right-hand side of (2.40*b*) is no longer subdominant.

## 9. Concluding remarks

We have addressed the deformation of a Skalak capsule under strong uniaxial elongation. The desire to employ slender-body theory has been impeded by two obstacles. The first is that the slender geometry, and in particular the slenderness $\epsilon$, is unknown to begin with. This obstacle is quite familiar from classical analyses of deformable bubbles in such flows (Buckmaster 1972, 1973; Acrivos & Lo 1978; Sherwood 1981) as well as comparable investigations of both hydrostatic (Sherwood 1991; Stone, Lister & Brenner 1999; Rhodes & Yariv 2010) and hydrodynamic (Dubash & Mestel 2007; Yariv & Rhodes 2013) deformations under an electric field. It is handled by temporarily considering the shape to be known. The second obstacle, unique to membrane deformation, has to do with the intrinsic conflict between Lagrangian and Eulerian descriptions. In the present contribution, it was tackled via the use of the inverse of the standard mapping from the reference state.

The slender-body ansatz allows us to obtain elementary approximations for the elastic stresses in the membrane. Making use of the paradigm of Keller & Rubinow (1976), it also provides closed-form approximations for the hydrodynamic stresses. This approach eventually results in a reduced problem, consisting of (5.1) and (5.4) and conditions

(5.5*b*)–(5.8), governing two functions of the axial coordinate. The first is the net cross-sectional tension; the second is the above-mentioned inverse map. The asymptotic error in the reduced problem is algebraically small in $\epsilon$ (and therefore also in $Ca$). In solving it, however, we have eventually resorted to a 'logarithmic' approximation, neglecting terms of order $1/\ln\epsilon$. The shape prediction of the resulting closed-form solution is in surprising agreement with numerical results in the literature, obtained at rather mild values of the capillary number.

It would be of interest to solve the reduced problem numerically (Tornberg & Shelley 2004) and compare the results, where the asymptotic error is ensured to be algebraically small, to the logarithmic approximation derived herein. Another natural direction is motivated by the experimental observation of capsule breakup in strong flows (Barthés-Biesel 1991): for a given lytic tension, one could use the asymptotic results in the present contribution as a basis for rupture prediction (Dodson III & Dimitrakopoulos 2009), possibly allowing the identification of a critical capillary number. Also, given the instabilities that are encountered in numerical simulations, is is desirable to use the steady shape identified in the present contribution as a basis for a stability calculation, possibly allowing the identification of a critical capillary number.

Otherwise, future extensions of the present work fall into three categories. The first involves the limit of large capillary numbers with nearly inextensible membranes. As observed in § 8, our asymptotic analysis breaks down when $C$ becomes comparable to $\epsilon^{-4/3}$. Assuming that the scaling (3.16) is retained, this suggests the analysis of the distinguished limit where $Ca$ and $C$ are large with $C^{1/2}/Ca$ fixed.

The second category entails the same flow problem with a more sophisticated membrane model (Barthés-Biesel 2016). Perhaps the most important modification is the introduction of a small resistance to bending which necessarily follows from the small but finite membrane thickness. This modification is expected to be significant near the tips, where it excludes the possibility of cusped ends.

The third category involves the consideration of different ambient flows. Perhaps the most important direction in that category is the consideration of planar extensional flow. This flow has been ubiquitous in theoretical analysis (Dodson III & Dimitrakopoulos 2009), perhaps because of the feasibility of simple experimental realisation via a four-roller mill set-up (Bentley & Leal 1986). Since it results in a steady state, it is simpler to analyse than, say, shear flow. Nonetheless, the resulting problem is more challenging than the present one as it does not possess axial symmetry. In particular, the cross-sectional shape is not circular. This requires a more sophisticated use of slender-body theory (Batchelor 1970; Borker & Koch 2019).

**Acknowledgements.** We are grateful to D. Barthés-Biesel and C. Dupont (UMR CNRS 7338, Université de Technologie de Compiègne) for insightful discussions and for providing us with their recent numerical data. We thank the NSF for support from CBET-2246791 and NIH via the National Heart, Lung and Blood Institute under grant no. R01HL132906.

**Declaration of interests.** The authors report no conflict of interest.

## References

Acrivos, A. & Lo, T.S. 1978 Deformation and breakup of a single slender drop in an extensional flow. *J. Fluid Mech.* **86** (4), 641–672.

Barthés-Biesel, D. 1980 Motion of a spherical microcapsule freely suspended in a linear shear flow. *J. Fluid Mech.* **100** (4), 831–853.

Barthés-Biesel, D. 1991 Role of interfacial properties on the motion and deformation of capsules in shear flow. *Physica A: Stat. Mech. Applics* **172** (1–2), 103–124.

BARTHÉS-BIESEL, D. 2016 Motion and deformation of elastic capsules and vesicles in flow. *Annu. Rev. Fluid Mech.* **48** (1), 25–52.

BARTHÈS-BIESEL, D., DIAZ, A. & DHENIN, E. 2002 Effect of constitutive laws for two-dimensional membranes on flow-induced capsule deformation. *J. Fluid Mech.* **460**, 211–222.

BARTHÉS-BIESEL, D. & RALLISON, J.M. 1981 The time-dependent deformation of a capsule freely suspended in a linear shear flow. *J. Fluid Mech.* **113** (−1), 251–267.

BATCHELOR, G.K. 1970 Slender-body theory for particles of arbitrary cross-section in stokes flow. *J. Fluid Mech.* **44** (3), 419–441.

BENTLEY, B.J. & LEAL, L.G. 1986 An experimental investigation of drop deformation and breakup in steady, two-dimensional linear flows. *J. Fluid Mech.* **167**, 241–283.

BOOTY, M.R. & SIEGEL, M. 2005 Steady deformation and tip-streaming of a slender bubble with surfactant in an extensional flow. *J. Fluid Mech.* **544**, 243–275.

BORKER, N.S. & KOCH, D.L. 2019 Slender body theory for particles with non-circular cross-sections with application to particle dynamics in shear flows. *J. Fluid Mech.* **877**, 1098–1133.

BUCKMASTER, J. 1973 The bursting of pointed drops in slow viscous flow. *J. Appl. Mech.* **40** (1), 18–24.

BUCKMASTER, J.D. 1972 Pointed bubbles in slow viscous flow. *J. Fluid Mech.* **55** (03), 385–400.

CHANG, K.-S. & OLBRICHT, W.L. 1993 Experimental studies of the deformation of a synthetic capsule in extensional flow. *J. Fluid Mech.* **250**, 587–608.

COX, R.G. 1970 The motion of long slender bodies in a viscous fluid Part 1. General theory. *J. Fluid Mech.* **44** (04), 791–810.

DODSON, W.R., III & DIMITRAKOPOULOS, P. 2008 Spindles, cusps, and bifurcation for capsules in stokes flow. *Phys. Rev. Lett.* **101** (20), 208102.

DODSON, W.R., III & DIMITRAKOPOULOS, P. 2009 Dynamics of strain-hardening and strain-softening capsules in strong planar extensional flows via an interfacial spectral boundary element algorithm for elastic membranes. *J. Fluid Mech.* **641**, 263–296.

DOWELL, E.H. & HALL, K.C. 2001 Modeling of fluid-structure interaction. *Annu. Rev. Fluid Mech.* **33** (1), 445–490.

DUBASH, N. & MESTEL, A.J. 2007 Behaviour of a conducting drop in a highly viscous fluid subject to an electric field. *J. Fluid Mech.* **581**, 469–493.

DUPONT, C. & BARTHÉS-BIESEL, D. 2024 Private communication, UMR CNRS 7338. Université de Technologie de Compiègne.

EGGLETON, C.D. & POPEL, A.S. 1998 Large deformation of red blood cell ghosts in a simple shear flow. *Phys. Fluids* **10** (8), 1834–1845.

FRAENKEL, L.E. 1969 On the methods of matched asymptotic expansions. Part I: a matching principle. *Math. Proc. Camb. Phil. Soc.* **65** (1), 209–231.

HINCH, E.J. & ACRIVOS, A. 1979 Steady long slender droplets in two-dimensional straining motion. *J. Fluid Mech.* **91** (03), 401–414.

KELLER, J.B. & RUBINOW, S.I. 1976 Slender-body theory for slow viscous flow. *J. Fluid Mech.* **75** (04), 705–714.

LI, X.Z., BARTHÉS-BIESEL, D. & HELMY, A. 1988 Large deformations and burst of a capsule freely suspended in an elongational flow. *J. Fluid Mech.* **187**, 179–196.

MIETKE, A., OTTO, O., GIRARDO, S., ROSENDAHL, P., TAUBENBERGER, A., GOLFIER, S., ULBRICHT, E., ALAND, S., GUCK, J. & FISCHER-FRIEDRICH, E. 2015 Extracting cell stiffness from real-time deformability cytometry: theory and experiment. *Biophys. J.* **109** (10), 2023–2036.

NAVOT, Y. 1998 Elastic membranes in viscous shear flow. *Phys. Fluids* **10** (8), 1819–1833.

OTTO, O., *et al.* 2015 Real-time deformability cytometry: on-the-fly cell mechanical phenotyping. *Nat. Meth.* **12** (3), 199–202.

POZRIKIDIS, C. 1990 The axisymmetric deformation of a red blood cell in uniaxial straining stokes flow. *J. Fluid Mech.* **216**, 231–254.

POZRIKIDIS, C. 2003*a* Deformed shapes of axisymmetric capsules enclosed by elastic membranes. *J. Engng Math.* **45** (2), 169–182.

POZRIKIDIS, C. 2003*b* *Modeling and Simulation of Capsules and Biological Cells*. Chapman & Hall.

RAMANUJAN, S. & POZRIKIDIS, C. 1998 Deformation of liquid capsules enclosed by elastic membranes in simple shear flow: large deformations and the effect of fluid viscosities. *J. Fluid Mech.* **361**, 117–143.

RHODES, D. & YARIV, E. 2010 The elongated shape of a dielectric drop deformed by a strong electric field. *J. Fluid Mech.* **664**, 286–296.

ROSENDAHL, P. *et al.* 2018 Real-time fluorescence and deformability cytometry. *Nat. Meth.* **15** (5), 355–358.

SHERWOOD, J.D. 1981 Spindle-shaped drops in a viscous extensional flow. *Math. Proc. Camb. Phil. Soc.* **90** (3), 529–536.

SHERWOOD, J.D. 1991 The deformation of a fluid drop in an electric field: a slender-body analysis. *J. Phys. A: Math. Gen.* **24** (17), 4047–4053.

SKALAK, R., TOZEREN, A., ZARDA, R.P. & CHIEN, S. 1973 Strain energy function of red blood cell membranes. *Biophys. J.* **13** (3), 245–264.

STONE, H.A., LISTER, J.R. & BRENNER, M.P. 1999 Drops with conical ends in electric and magnetic fields. *Proc. R. Soc. Lond. A* **455**, 329.

TILLETT, J.P.K. 1970 Axial and transverse Stokes flow past slender axisymmetric bodies. *J. Fluid Mech.* **44** (3), 401–418.

TORNBERG, A.-K. & SHELLEY, M.J. 2004 Simulating the dynamics and interactions of flexible fibers in Stokes flows. *J. Comput. Phys.* **196** (1), 8–40.

VAN DYKE, M. 1964 *Perturbation Methods in Fluid Mechanics*. Academic Press.

WALTER, J., SALSAC, A.-V., BARTHÈS-BIESEL, D. & LE TALLEC, P. 2010 Coupling of finite element and boundary integral methods for a capsule in a Stokes flow. *Intl J. Numer. Meth. Engng* **83** (7), 829–850.

WANG, Y. & DIMITRAKOPOULOS, P. 2006 A three-dimensional spectral boundary element algorithm for interfacial dynamics in Stokes flow. *Phys. Fluids* **18** (8), 082106.

YARIV, E. & RHODES, D. 2013 Electrohydrodynamic drop deformation by strong electric fields: slender-body analysis. *SIAM J. Appl. Math.* **73** (6), 2143–2161.